



**HAL**  
open science

# The impact of Storm Alex on the Vievola catchment: a quantitative analysis of sediment volume and morphological changes in the Roya River tributaries

Raphaël Kerverdo, Sara Lafuerza, Christian Gorini, Alain Rabaute, Didier Granjeon, Rémy Deschamps, Eric Fouache, Mina Jafari, Pierre-Yves Lagrée

## ► To cite this version:

Raphaël Kerverdo, Sara Lafuerza, Christian Gorini, Alain Rabaute, Didier Granjeon, et al.. The impact of Storm Alex on the Vievola catchment: a quantitative analysis of sediment volume and morphological changes in the Roya River tributaries. *Landslides*, 2024, 10.1007/s10346-024-02361-2 . hal-04708457

**HAL Id: hal-04708457**

**<https://hal.science/hal-04708457v1>**

Submitted on 30 Sep 2024

**HAL** is a multi-disciplinary open access archive for the deposit and dissemination of scientific research documents, whether they are published or not. The documents may come from teaching and research institutions in France or abroad, or from public or private research centers.

L'archive ouverte pluridisciplinaire **HAL**, est destinée au dépôt et à la diffusion de documents scientifiques de niveau recherche, publiés ou non, émanant des établissements d'enseignement et de recherche français ou étrangers, des laboratoires publics ou privés.

1 THE IMPACT OF STORM ALEX ON THE VIEVOLA CATCHMENT: A QUANTITATIVE  
2 ANALYSIS OF SEDIMENT VOLUME AND MORPHOLOGICAL CHANGES IN THE ROYA  
3 RIVER TRIBUTARIES

4 Raphaël KERVERDO<sup>1</sup> [raphael.kerverdo@sorbonne-universite.fr](mailto:raphael.kerverdo@sorbonne-universite.fr) [0009-0008-8984-0749](https://orcid.org/0009-0008-8984-0749), Sara LAFUERZA<sup>1</sup>  
5 [0000-0003-2126-6505](https://orcid.org/0000-0003-2126-6505), Christian GORINI<sup>1</sup> [0000-0003-3123-4822](https://orcid.org/0000-0003-3123-4822), Alain RABAUTE<sup>1</sup> [0000-0003-1369-0218](https://orcid.org/0000-0003-1369-0218),  
6 Didier GRANJEON<sup>2</sup> [0000-0002-1457-6671](https://orcid.org/0000-0002-1457-6671), Rémy DESCHAMPS<sup>2</sup> [0000-0002-0888-3456](https://orcid.org/0000-0002-0888-3456), Eric FOUACHE<sup>3</sup>  
7 [0000-0002-5392-0615](https://orcid.org/0000-0002-5392-0615), Mina JAFARI, Pierre-Yves LAGREE [0000-0002-3931-6622](https://orcid.org/0000-0002-3931-6622),

8 <sup>1</sup>*Institut des Sciences de la Terre de Paris (ISTeP), Sorbonne Université, CNRS-INSU, 75005 Paris, France*

9 <sup>2</sup>*IFP Energies Nouvelles, Rueil-Malmaison, France*

10 <sup>3</sup>*Laboratoire Médiations, Institut de Géographie, Sorbonne Université, Paris, France*

11 <sup>4</sup>*Institut Jean le Rond d'Alembert, Sorbonne Université, Paris, France*

12 Corresponding author : Raphaël KERVERDO [raphael.kerverdo@sorbonne-universite.fr](mailto:raphael.kerverdo@sorbonne-universite.fr)

13 Abstract

14 This study investigates the sediment dynamics resulting from the extreme storm Alex in October 2020 in the Roya  
15 Valley and its tributaries in the Alpes-Maritimes region, France. The storm, triggered by a low-pressure system,  
16 led to unprecedented rainfall, causing extensive flooding and erosion in the region. Despite limited pre-flood data,  
17 the study employs aerial and satellite imagery, digital elevation models, and field surveys to quantify sediment  
18 mobilization and its effects on the Viévolâ alluvial fan in the Roya Valley.

19 The Roya Valley's complex geomorphology, characterised by steep gradients, gullies, and torrential streams,  
20 played a significant role in sediment transport. The study reveals that the Dente and Rabay torrents were major  
21 sediment contributors, with gullies in these areas producing substantial erosion. Bank erosion in the Dente valley  
22 was particularly prominent, attributed to geological factors and glacial deposits.

23 The analysis, relying on topographical comparisons and digital data, assesses sediment volumes eroded and  
24 deposited during the event. Despite challenges in data quality, the study offers valuable insights into sediment  
25 dynamics during extreme hydro-sedimentary events. The Viévolâ catchment area is a focal point, emphasizing the  
26 importance of scree and fluvio-glacial deposits as primary sources of sediment.

27 The findings emphasize the need for improved pre-event data and monitoring in mountainous regions susceptible  
28 to extreme events. The study's methodology, despite limitations, contributes to a better understanding of  
29 geomorphic responses to extreme events. Expanding similar studies to cover a wider range of catchment areas and  
30 incorporating field data offers potential for enhanced hazard assessment and management strategies. The research  
31 underscores the critical role of sediment transport in shaping landscapes and impacting human infrastructure during  
32 extreme flood events.

33 Keywords: Storm Alex, torrent, flood, erosion, DoD, GIS

34 Statements and Declarations

35 The authors declare no conflicts of interest.

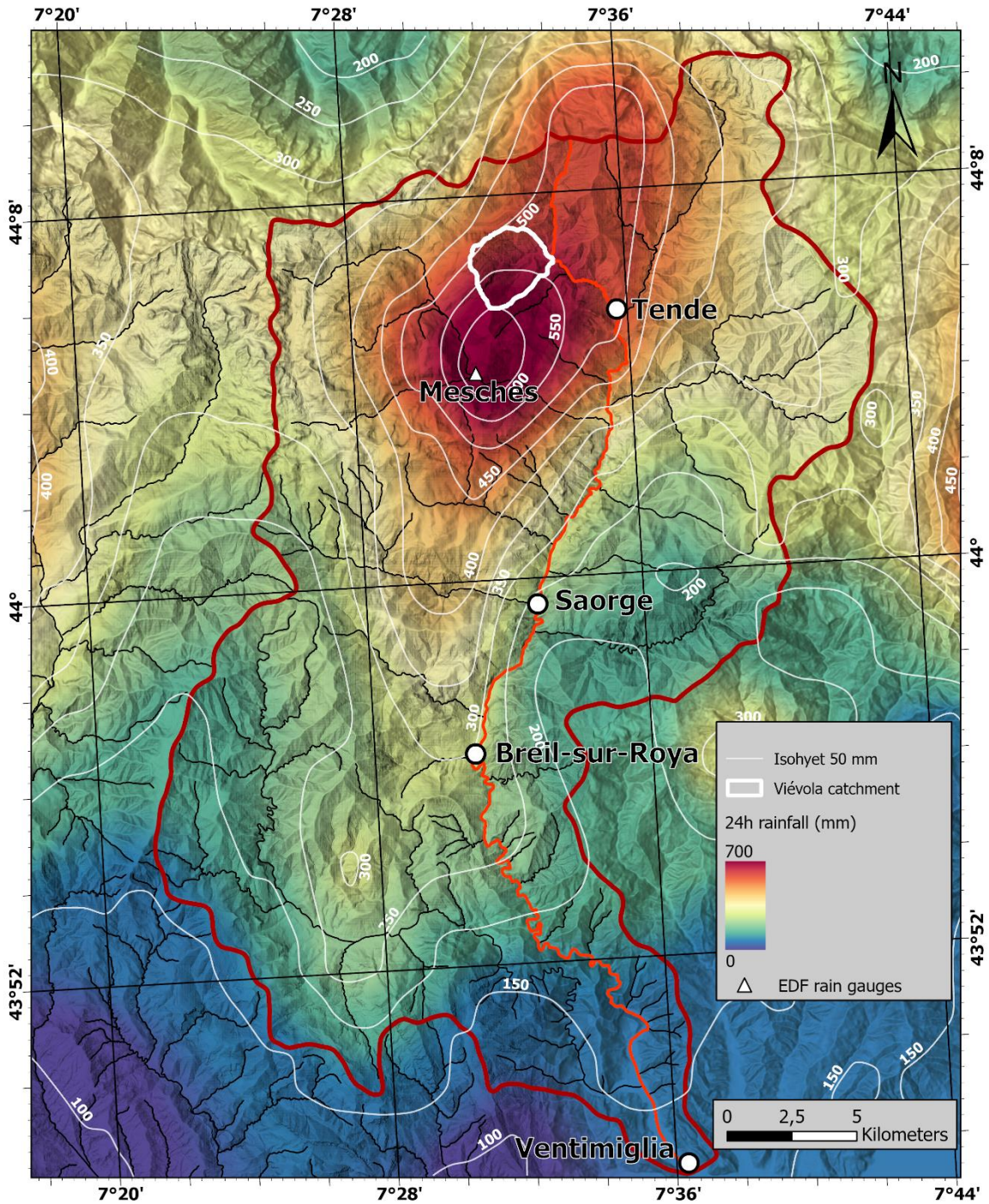
36

37

38

39 1. Introduction

40 The high valleys of the Tinée, Vésubie and Roya rivers were struck by the extreme storm Alex from mid-day on  
41 October 2<sup>nd</sup>, 2020 to the early morning of October 3<sup>rd</sup>. This storm was triggered by the rapid deepening of a low-  
42 pressure system over the Atlantic. The Alex storm reached the west coast of France the night of October 1<sup>st</sup>,  
43 generating a significant southern flux coming from the Mediterranean Sea. The warm and humid air mass from  
44 the Mediterranean Sea caused an exceptional Mediterranean rainfall episode in the Alpes-Maritimes hinterland  
45 (Figure 1), exceeding the 100-year return period rainfall for a 4-hour total and a 1000-year return period rainfall  
46 for a 12-hour total (Carrega and Michelot, 2021; Cerema, 2021; ONF-RTM, ONF-DRN, and INRAE-ETNA,  
47 2023). In the Roya Valley, the maximum cumulated rainfall in 24 hours was observed at Mesches dam at about  
48 663 mm (Cerema, 2021).



49 **Fig.1** :24 hr rainfall map in the Roya valley, as modified by Liébault et al. (2024). The catchment divide is highlighted in red,  
50 stream networks are depicted as thin black lines, and the Roya River is represented by a thick dark orange line. The Viévol  
51 catchment area is delineated in the upper part of the valley in light white.

53 Hydrological modelling of the Alex Storm, calibrated on the few available field observations, made it possible to  
 54 estimate the peak discharge of the Roya River between 1100 and 1800 m<sup>3</sup>/s at Breil-sur-Roya (Cerema, 2021).  
 55 These changes are detailed in Table 1, providing a clear picture of the impact of the storm on the valley based on  
 56 the work of Liébault et al. (2024)

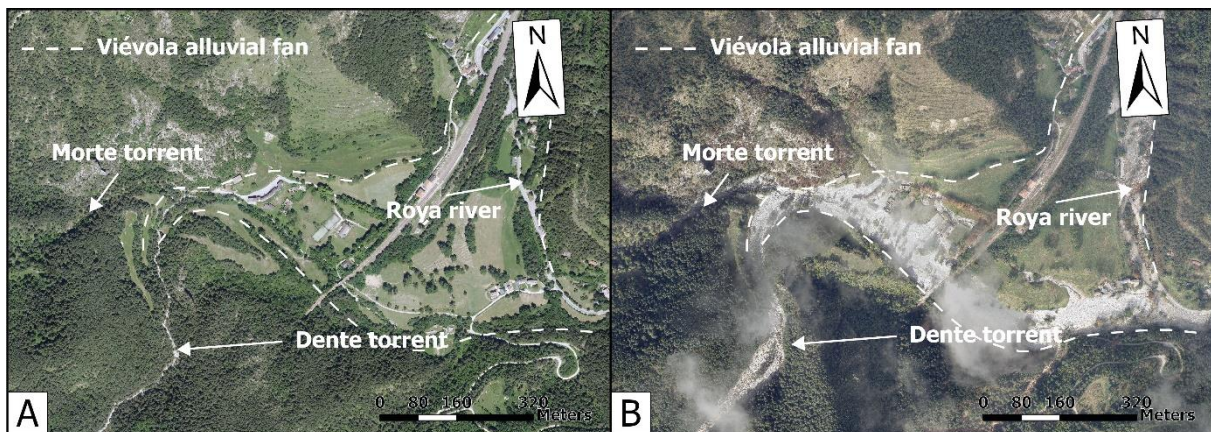
57 *Table 1. Summary of morphological changes and mobilized volumes for the Roya and Vésubie catchments as reported by*  
 58 *Liébault et al. (2024). The volumes were calculated using LiDAR data obtained by the Nice metropolitan authority in 2018. In*  
 59 *the case of the Roya valley, the unavailability of pre-flood LiDAR data hindered the determination of mobilized volumes. IC,*  
 60 *Index of Confinement, which is defined as the ratio between the post-active channel band and modern valley floor width.*

61

Vésubie							
Surface channel (ha)		Modern valley floor (ha)		Mean active channel (m)		IC (ratio)	
Before (2017)	After (2020)	Before (2018)	After (2020)	Before (2018)	After (2020)	76%	
68	274	317	363	19	79		
Total erosion		Total deposition		Tributaries input		Net budget exported	
Value	Uncertainties	Value	Uncertainties	Value	Uncertainties	Value	Uncertainties
4,13Mm <sup>3</sup>	0,011Mm <sup>3</sup>	3,49Mm <sup>3</sup>	0,016Mm <sup>3</sup>	1,51Mm <sup>3</sup>	0,025Mm <sup>3</sup>	2,06Mm <sup>3</sup>	0,050Mm <sup>3</sup>
Roya							
Surface channel (ha)		Modern valley floor (ha)		Mean active channel (m)		IC (ratio)	
Before (2017)	After (2020)	Before	After (2020)	Before (2017)	After (2020)	75%	
59	137	Unknown	181	15	37		
Total erosion		Total deposition		Tributaries input		Net budget exported	
Unknown		Unknown		Unknown		Unknown	

62

63 Our work presents the methodology for quantifying the mobilised sediment during the Storm Alex in one of the  
 64 most active tributary systems of the Roya Valley, namely the Viévolâ alluvial fan (Figures 1 and 2) and discuss  
 65 the impact of the data availability on quantifying erosion and sediment transport for hazard assessment. The flatter  
 66 landforms developed in alluvial fans, such as the Viévolâ fan elevated above the Roya floodplain, are attractive  
 67 for site developments, such as camp resorts (Figure 2-A). The activity recorded in the Viévolâ alluvial fan  
 68 highlights how these sedimentary systems can severely impact human activity during extreme floods (Figure 2-  
 69 B).



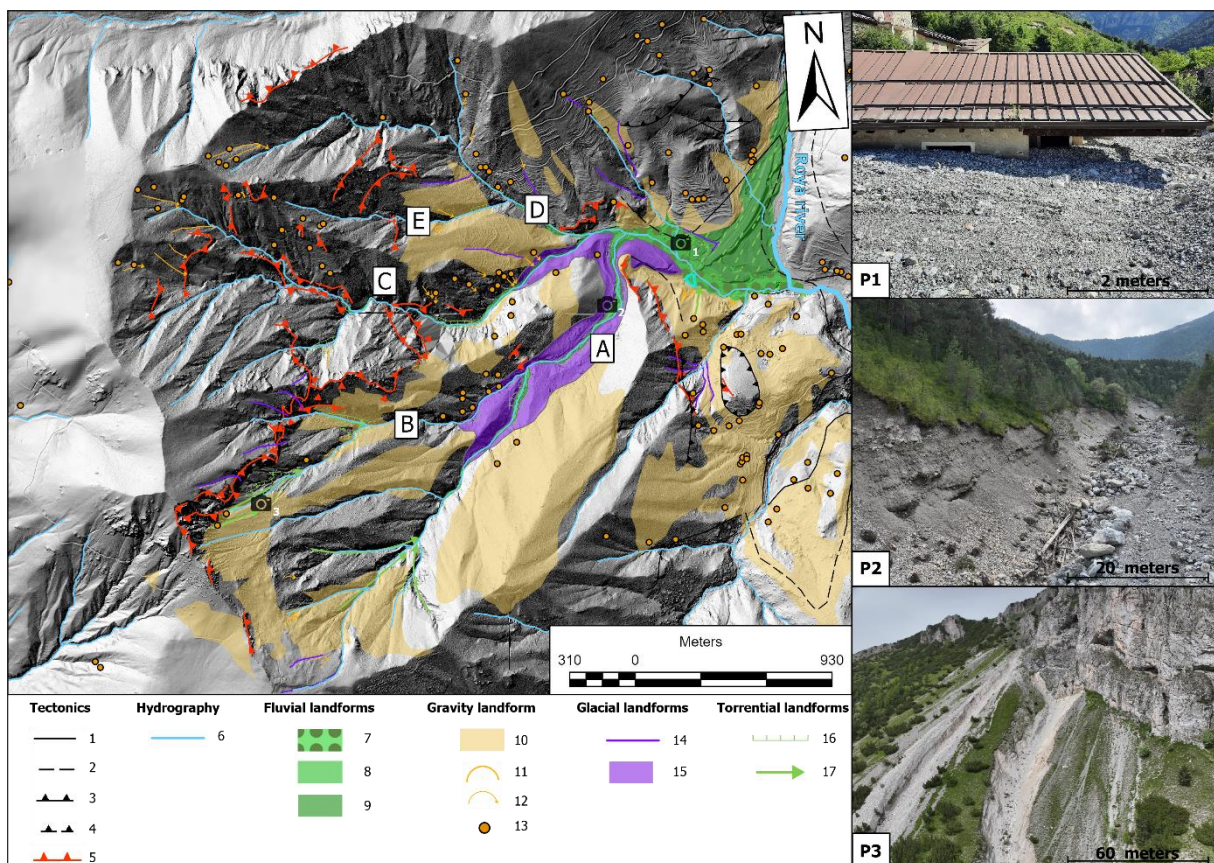
70 **Fig. 2 :** The Viévolâ resort camp is depicted in two snapshots, showcasing the conditions before and after the October 2020  
 71 flood. In the post-flood image, the torrents and the Roya River on the right side of the picture exhibit significant changes, with  
 72 noticeable increases in depth and width. The southern part of the Viévolâ alluvial fan was heavily embanked following the  
 73 flood.

## 74 2. Study area

75 The Roya subalpine valley (Figure 1) encompasses a watershed of 671 km<sup>2</sup> bordered in the North by the Argentera-  
 76 Mercantour massif (elevations up to 3000 m) and the Col de Tende (1889 a.s.l). The Roya River extends 60 km in  
 77 a north to south direction, flowing into the Mediterranean Sea. Its valley exhibits a V-shaped forming significant  
 78 gorges that channel the river for much of its course (Blanchard, 1949; Julian, 1980). The average valley gradient

79 is about 56% (ONF-RTM, ONF-DRN, and INRAE-ETNA, 2023). Its morphology characterised by a step-pool  
 80 channel is primarily fed by gullies and torrents that incise the valley slopes. The lithology of the region, mainly  
 81 comprising competent rocks such as a Jurassic/Cretaceous marls and limestones, contributes to these  
 82 morphologies. Alluvial terraces and fans mobilising fluvio-glacial materials are found as the valley widens, notably  
 83 at the Viévolle alluvial fan (Figure 2) at the confluence of the Morte and Roya rivers, and at Saint-Dalmas-de-  
 84 Tende at the confluence of the Bieugne and Roya rivers. The Bieugne river flows downstream the Mesches dam  
 85 were the highest rainfall recorded (Figure 2).

86 The Viévolle fan covering an area of 6.5 km<sup>2</sup>, evolves where the Morte and Dente torrents deconfine and flow into  
 87 the right bank of the Roya River (Figure 2). The morphology of this watershed (Figure 3- A) has a radial shape  
 88 sculpted by the last glaciation (Julian, 1997; Brisset *et al.*, 2015). This area is divided into five valleys : the Dente,  
 89 Rabay, Morte, Para and Scabrie valleys (Figure 2). The Dente torrent with a length of 1.8 km, converges with the  
 90 Morte torrent at the apex of the Viévolle alluvial fan. The Rabay torrent, 1.4 km long, serves as a tributary to the  
 91 Dente torrent. The longest of these is the Morte, stretching 2.5 km. The Para and Scabrie torrents feed into the  
 92 Morte, each 1.4 km and 1.1 km long respectively. Torrent gradients exceed 30°. The unconsolidated rocks within  
 93 the Roya catchment primarily comprise scree slopes and aprons located on the slopes of different torrents, as  
 94 shown in Figure 3-A. Notably, the downstream segments of the Dente and Morte torrents are characterised by  
 95 glacial outwash deposits (ONF-RTM, ONF-DRN, and INRAE-ETNA, 2023).



96 **Fig. 3:** A - Left. Geomorphological map of the Viévolle catchment area. Data was combined with the 1:50,000 BRGM map  
 97 (Gèze and Nesteroff, 1996) and reports from the ONF, RTM and INRAE. A) Vallon de Dente B) Vallon de Rabay C) Vallon de  
 98 Morte D) Vallon de Para and E) Vallon de Scabrie. 1- Fault ; 2- Supposed fault ; 3- Thrust ; 4- Supposed Thrust ; 5- Rocky  
 99 escarpment ; 6- Rivers / torrents ; 7- Alluvial fan (Alex 2020) ; 8- Fluvial accumulation ; 9- Alluvial fan (Pléistocene) ; 10-  
 100 Scree ; 11- Scarps ; 12- Scree corridor ; 13- Landslides ; 14- Glacial striae ; 15- Fluvio-glacial outwash ; 16- Torrential  
 101 scarp ; 17- Major gully. B : Photo 1 - Alex flood debris flows engraving one of the buildings of the Viévolle camp resort  
 102 during the Alex storm flood (5th July 2021). Photo 2 – Dente torrent after the flood, on the left side we can see the glacial  
 103 fluvial outwash deposits. Photo 3 – Major gullies observed at the headwaters of the Rabay area.

### 104 3. Data

105 A range of data sets including aerial and infrared pictures and digital elevation models covers the pre-flood and  
 106 post-flood periods. Following Alex flood, the IGN (Institut Géographique National, French geographical survey)

107 conducted an emergency survey with aerial orthoimages and LiDAR images covering the major river floors of the  
108 Tinée, Vésubie and Roya valleys (IGN, 2020). The post-Alex LIDAR 2020 has a planimetric resolution of 0.5m  
109 and altimetric resolution of 0.3m corresponding to the IGN's NUALID LiDAR (less than 10 points per m<sup>2</sup>). In  
110 June 2021, IGN collected new LiDAR HD images (point density > 10 points per m<sup>2</sup>) for the Alpes-Maritimes as  
111 part of the national LiDAR coverage programme (IGN, 2021). In ArcGIS Pro 3.1.2 (ESRI Inc.), two sets of point  
112 clouds have been classified to generate a Digital Terrain Model,  $DTM_{2021}$  and a Digital Surface Model,  $DSM_{2021}$ .  
113 The  $DTM_{2021}$  and  $DSM_{2021}$  have a planimetric resolution of 0.5m and an altimetric resolution of 0.1m (IGN,  
114 2023a). A Digital Terrain Model (DTM) provides information about the elevation of terrain features, typically  
115 represented as a grid of elevation values. A Digital Surface Model (DSM) includes the elevations of natural and  
116 artificial features, such as trees, buildings, and other structures. It provides a detailed and accurate depiction of the  
117 terrain's topography, including surface features.

118 The Roya Valley's latest (pre-flood) digital terrain model (RGE Alti ®) dates from 2008 and is of poor quality for  
119 mountainous areas. In fact, radar acquisitions have been favoured in mountainous and steeply sloping areas,  
120 reducing altimetric accuracy to an average of 7m (IGN, 2018). Only valley floors were imaged with acceptable  
121 resolutions, although they are not helpful for in steeply sloping areas. Before October 2020, no LiDAR images  
122 cover the entire Roya Valley.

123 The only good quality data prior to the event is the correlated digital surface model ("MNS Correl" produced by  
124 IGN), which has an altimetric error of +/- 0.2m (IGN, 2023). The Correl DSM is a regular grid of altitudes  
125 representing the ground or surface without differentiation obtained through the correlation of aerial images. The  
126 correlation is a process that automatically detects corresponding points between different captures of the same  
127 scene. The intersection of these corresponding beams, thus reconstructed, allows deducing the XYZ coordinates  
128 of the point in the scene (IGN, 2023). This raster, named herein  $DSM_{2020}$ , constitutes our reference before the  
129 flood and will be compared with the LiDAR dataset acquired after event  $DTM_{2021}$ .

130 The cumulative altimeter error for  $DSM_{2020}$  and  $DTM_{2021}$  is within the range of +/- 0.3m range.

131 In addition, several drone surveys were carried out in March, June and October 2023 (Figure 3-B, Photo 2) in the  
132 Viévol catchment area, with a DJI Mavic 3<sup>E</sup> including a RTK module and an Orpheon subscription (enabling  
133 correct geo-referencing for the orthoimages). Photogrammetric models were processed with Agisoft Metashape  
134 1.8.3 Pro software and exported to ArcGIS Pro 3.1.2 (ESRI Inc.) to map the eroded and transported sediments and  
135 volume quantification.

#### 136 4. Methodology

137 To ascertain the sediment volumes eroded and deposited within the Viévol catchment area, we employed the  
138  $DSM_{2020}$  as our pre-Alex data and the  $DTM_{2021}$  for the post-Alex assessment. Despite the  $DTM_{2021}$  dataset being  
139 acquired eight months subsequent to the post-Alex LIDAR 2020, it was deemed more suitable owing to its higher  
140 resolution. The post-Alex 2020 data (raw LiDAR NUALID) necessitated calibration, noise reduction and  
141 correction for ellipsoidal height, a process not requisite for the  $DTM_{2021}$ . Notably, no significant changes happened  
142 during the time lapse after the Alex flood and July 2021 since the period was characterised by very low  
143 precipitations (see supplementary data). Herein, the sediment volumes that are eroded and transported are  
144 considered **Ground erosion**.

145 For volume determination, we initially performed a topographical comparison (Equation 1) :

$$146 \quad DTM_{2021} - DSM_{2020} = \Delta DSM \quad (1)$$

147 The  $\Delta DSM$  denotes the altimetric difference between the two datasets. In areas impacted by the storm, the  $\Delta DSM$   
148 provides insights into the total erosion during the flood (Figure 4), encompassing both the canopy height and the  
149 eroded ground thickness. In vegetation-free areas, the  $\Delta DSM$  exclusively represents the soil ground (Figure 4).  
150 For areas unaffected by the storm, the canopy height is indicated. Total erosion in vegetated areas is formulated as  
151 (Equation 2) :

$$152 \quad \Delta DSM = \text{"Tree cover thickness"} + \text{Ground erosion} \quad (2)$$

153 Equation 1 can extract ground erosion from the  $\Delta DSM$  by employing the average canopy height (i.e., tree cover)  
154 in flood-affected areas. As a result, Ground erosion in flood-impacted zones is isolated. From Equation 2, we can  
155 define the **Ground erosion** as:

$$156 \quad \text{Ground erosion} = \Delta DSM - \text{"Tree cover thickness"} \quad (3)$$

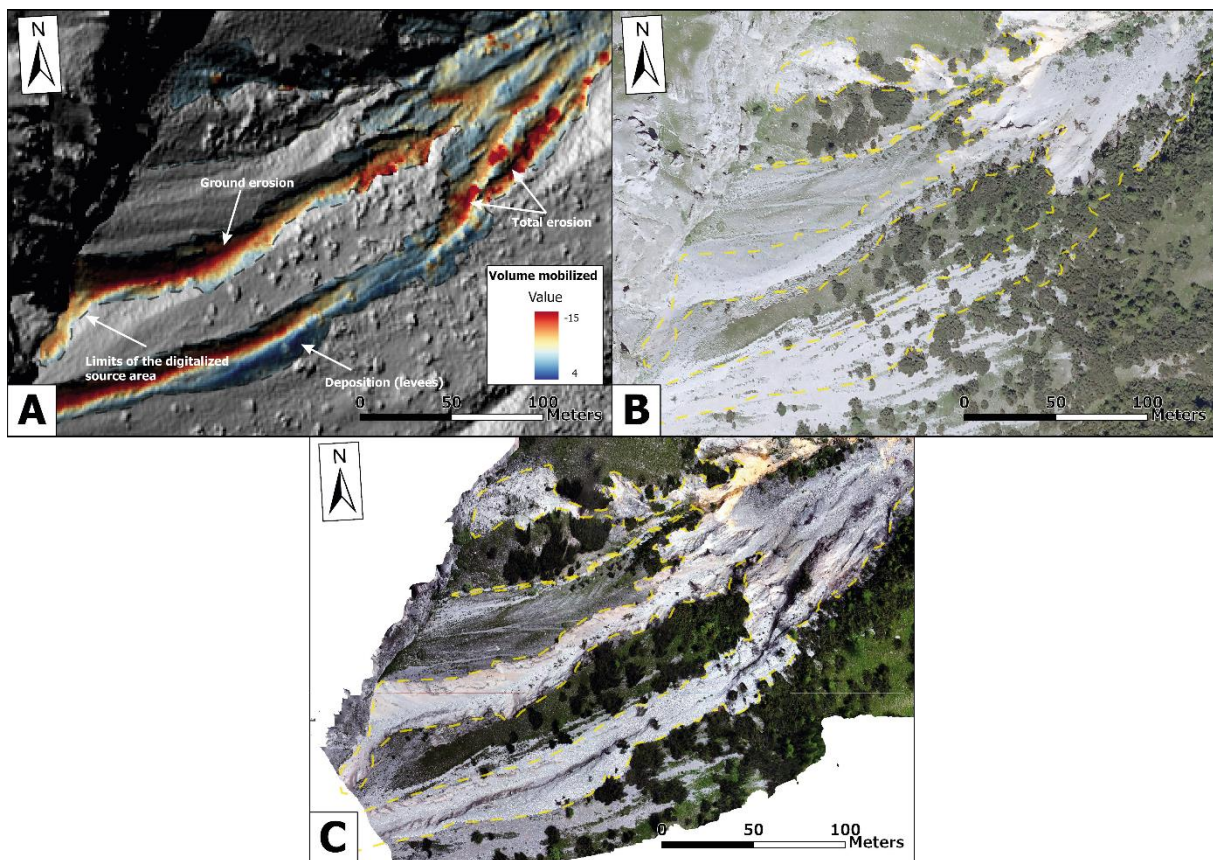
157 Herein, “tree cover thickness” pertains to the height of trees uprooted during Storm Alex, determined by deducting  
158 an average tree height from the  $DSM_{2020}$ .

159 This brings us to determine two zones of interest :

- 160 i) low vegetation zone (0-0.5m, according to IGN, 2023) where the surface of the DSM corresponds to  
161 the surface of the DTM. This can be expressed as follows from equation 1 : **Ground erosion** =  
162  $\Delta DSM$  with tree cover thickness = 0.  
163 ii) vegetated zone (>0.5m) where we know the total erosion i.e  $\Delta DSM$  (Eq. 1)

164 Before determining the mobilised volumes, we verified that the altimetric information in the  $DSM_{2020}$  the same as  
165 that in the  $DSM_{2021}$ . First, we calibrate the  $DSM_{2020}$  with respect to the  $DSM_{2021}$  (The  $DSM_{2021}$  is taken as the  
166 reference because it has the best resolution and the smallest altimetric error margin) in low vegetated zones and  
167 vegetated zones unaffected by storm Alex. We obtain -0.21m for low vegetated zones and -1.97m for all vegetated  
168 slopes in the watershed. To be more precise, this calibration difference has been estimated at the scale of each sub-  
169 valley of the studied torrent (see supplementary data). The negative value indicates an elevation of the  $DSM_{2020}$   
170 compared to the  $DSM_{2021}$ .

171



172 **Fig.4** : Illustration of altimetric differences at the head of the Rabay valley gullies ( $DTM_{2021} - DSM_{2020}$ ) across different  
173 temporal scales: A)  $DSM_{2021}$  post-flood B) orthoimages from July 2020 (pre-flood) C) orthoimages from October 5 to 7, 2020  
174 post-flood. A) Overlaid with the outcome of equation (1), delineating erosion zones (in red) and deposition zones (in blue). The  
175 delineated working area is marked by the dashed yellow line. In these visuals, we can observe areas with sparse vegetation  
176 where  $DSM_{2020}$  equals  $DTM_{2021}$ , allowing for direct estimation of **ground erosion**. Total erosion is notably pronounced in  
177 certain areas, reaching maximum values of up to -15m.

178 In order to distinguish tall vegetation, primarily trees in the vegetated area, we selected areas unaffected by Storm  
179 Alex from false-color composite images (BD Ortho IRC) produced by IGN for the Alpes-Maritimes in 2017. The  
180 IGN's IRC operates on three bands, the first corresponding to the NIR, the second to the red band and the third to  
181 the green band. NDVI (Normalized Difference of Vegetation Index) indices were calculated using the two first  
182 bands of false-color composite images. The fundamental principle of NDVI is that healthy vegetation absorbs  
183 most of visible light for photosynthesis (Tucker, 1979; Sellers, 1987) while reflecting a significant portion of near-  
184 infrared light. Sparse and unhealthy vegetation, on the other hand, reflects more visible light and less near-infrared  
185 light. By measuring the difference in reflectance between red and near-infrared bands, NDVI provides information

186 about vegetation health and density. The NDVI is calculated using the following formula Equation 3 :  $NDVI =$   
 187  $\frac{(NIR - Red)}{(NIR + Red)}$ .

188 Where NIR represents reflectance in the near-infrared band, and red represents reflectance in the red band. Values  
 189 range from -1 to 1, with negative values corresponding to water. Values near 0.1 indicate bare soil, snow, or sand,  
 190 an index between 0.2 – 0.3 corresponds to grasslands and bushes, and between 0.6 and 0.8 corresponds to tropical  
 191 forests (Holben, 1986).

192 In order to identify trees and the distribution of tree heights, we established an arbitrary vegetation detection  
 193 threshold based on (Derrien *et al.*, 1992) of >0.30 (see supplementary data). For each studied torrent (Figure 2),  
 194 we extract the height of trees on their slopes using the method outlined above and estimate an average height after  
 195 recalibration on the basis of the difference in elevation between  $DSM_{2021}$  and  $DSM_{2020}$  given in Table 2. The height  
 196 of these trees is employed for subtraction from the  $DSM_{2020}$  (Table 3).

197 For the volumes deduced from Equation 1, an error margin of  $\pm 0.3m$  is applied.

198 *Table 2 : The average tree heights were obtained after recalibrating the data using the methodology outlined above. Only the*  
 199 *valleys of Dente, Rabay, and Morte were considered, as they have clearly identifiable source zones (landslides, ravines), unlike*  
 200 *the Para and Scabrie torrents.*

	Dente	Rabay	Morte
Average height trees	10,6 +/- 0.3m	9,2 +/- 0.3m	9,5 +/- 0.3m

201  
 202 This methodology is applied in two major erosion zones : i) source areas such as gullies and landslides and ii) bank  
 203 erosion. It is also applied to the Viévolá alluvial fan to determine deposited volumes. This approach allows us to  
 204 estimate a sediment volume balance between the source (erosion) and deposition zones.

## 205 5. Results and discussions

206 The volumes eroded within the five torrents in the Viévolá catchment are presented in Table 3. Erosion related to  
 207 the event in these torrents is divided into three categories (gullies, bank erosion, and landslides), as explained  
 208 above with their associated error margins. The transport of the mobilised volumes (Table 3) results in a total  
 209 volume deposited in the Viévolá alluvial fan of  $88\,500m^3 \pm 19\,670\,m^3$  (Figure 5).

210 *Table 3 : Volumes eroded within the five torrents in Viévolá catchement during the Alex storm. Each erosion value holds the*  
 211 *uncertainties defined using the previous methodology. A total of  $179\,431\,m^3$  of sediments were released during the flood. The*  
 212 *total surfaces studied for the gullies volumes is  $67\,210\,m^2$ , for banks erosion is  $27\,444m^2$  and landslides is  $8\,733\,m^2$ . The last*  
 213 *line corresponds to the ratio between the eroded volumes and the surface area.*

Names	Gullies volumes		Banks erosion		Landslides		Total	
	Erosion ( $m^3$ )	Margin error ( $m^3$ )	Erosion ( $m^3$ )	Margin error ( $m^3$ )	Erosion ( $m^3$ )	Margin error ( $m^3$ )	Erosion ( $m^3$ )	Margin error ( $m^3$ )
<b>Dente torrent</b>	36 900	4 059	57 200	3 040	802	240	94 900	7 340
<b>Rabay torrent</b>	46 000	7 366	2 720	250	656	197	49 420	7 813
<b>Morte torrent</b>	14 000	3 100	--	--	16 700	5 004	30 644	8 107
<b>Para torrent</b>	--	--	--	--	3 800	1 140	3 800	1 140
<b>Scabrie torrent</b>	--	--	--	--	667	200	667	200
<b>Total</b>	96 900	14 525	59 920	3 290	22 625	6 781	179 431	24 600
<b>Surfaces (<math>m^2</math>)</b>	67 210		27 444		8 733		103 387	
$\frac{m^3}{m^2}$	1.4 m		2.1 m		2.6m		1.7 m	



214 The main contribution in sediment came from the Dente and Rabay Valleys (Table 3), totalling approximately 144  
215 300 m<sup>3</sup> (80% of the total erosion) with a margin of error of approximately 15 000 m<sup>3</sup>. Notably, the heads of the  
216 gullies in the Dente and Rabay valleys, situated in unconsolidated scree slopes, produced between 36 900 m<sup>3</sup> and  
217 46 000 m<sup>3</sup>, respectively (Table 3, Figure 4).

218 The Dente valley is characterised by significant bank erosion, contributing 57 200 m<sup>3</sup> of sediment (31% of the  
219 total erosion). Landslides made a negligible contribution of 802 m<sup>3</sup> (Table 3) and 656 m<sup>3</sup> in the Dente and Rabay,  
220 respectively. The ratios yield the following results: 1.4m for ravines, 2.1m for bank erosion, and 2.6m for  
221 landslides. Landslides have the highest ratio compared to ravines. Notably, the sediment contribution from the  
222 banks was particularly significant, with a ratio exceeding 2m. The contrast in bank erosion between these valleys  
223 can be attributed to two main factors.

224 Firstly, the Rabay River features a by-pass zone with a slope of around 30° where deposition is not feasible, and  
225 Jurassic/Cretaceous limestone is outcropping. Bank erosion is prominent at the exit downstream of the bypass  
226 zone, several hundred meters upstream of the confluence with the Dente torrent, where the gradient becomes  
227 milder (Figures 2 and 4). The second factor is the presence of glacial outwash deposits (Figure 2) associated with  
228 the last glaciation and/or the Little Ice Age (Julian, 1997; Brisset et al., 2015; ONF-RTM, ONF-DRN, and INRAE-  
229 ETNA, 2023). As depicted in Figure 2, the downstream section of the Dente torrent is composed of this  
230 unconsolidated lithology. The observed deposits on the Viévol alluvial fan correspond to cryoclastic deposits  
231 (Figure 3 – P1), reinforcing the notion of substantial erosion of fluvio-glacial outwash deposits.

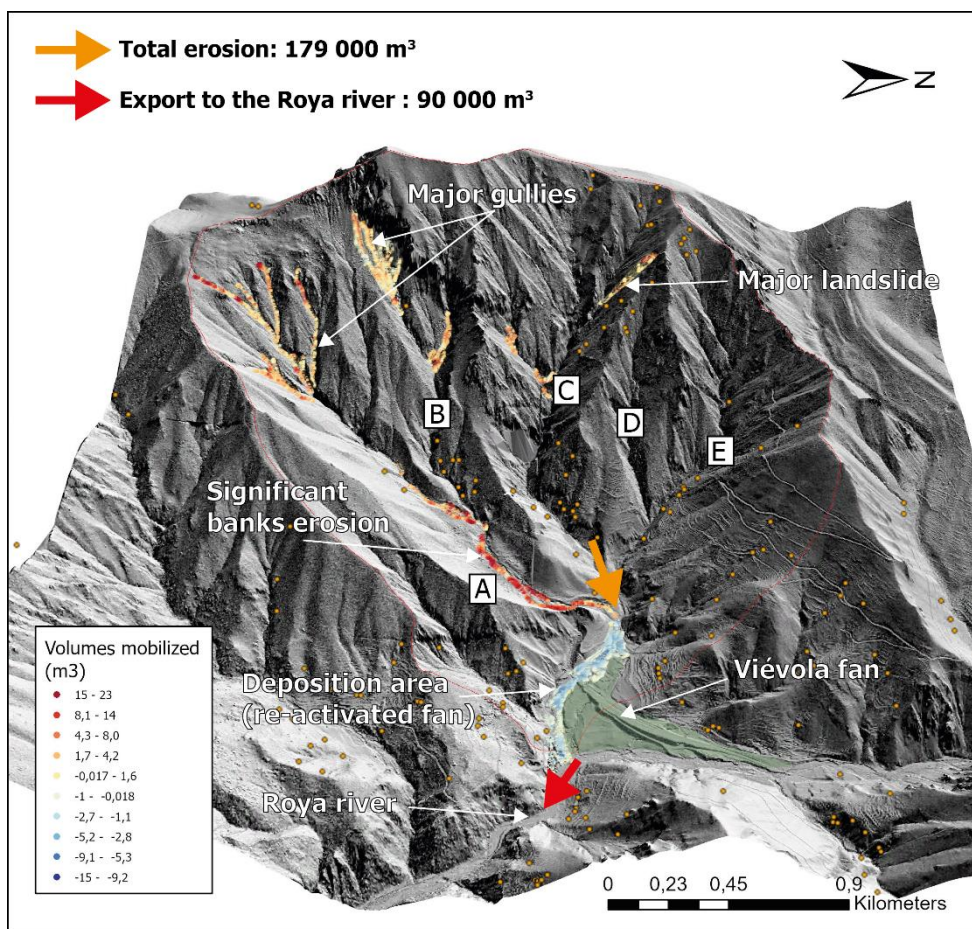
232 Sedimentary analysis of the deposits in the Dente torrent reveals a succession of debris flows characterised by  
233 typical sedimentary fronts and deposits. The force of such a flow is assumed to allow increased erosion of  
234 unconsolidated deposits (Figure 3 – P2), which, in this case, are the source of this substantial input from the banks  
235 of the Dente Valley (Figure 5).

236 The Morte, Para, and Scabrie torrents have produced less sediment (Table 3 and Figure 5). This may be explained  
237 by the fact that these valley heads lack large gullies, unlike the Dente and Rabay valleys (Figure 2 and P3 in Figure  
238 3). Notably, the heads of these sub-catchments do not feature scree slopes (Figure 2). However, there is a higher  
239 density of landslides. A significant landslide of approximately 13 000 m<sup>3</sup> occurred at the head of the Morte torrent  
240 (Figure 5), accounting for 54% of the sediment release upstream of this tributary. There is a apparent disparity in  
241 the contributions that landslide processes provide.

242 Orthoimages produced by IGN before and after the event reveal that most of the contributions from the Scabrie,  
243 Para, and Morte torrents are linked to the widening of the channel, indicating significant lateral erosion, though  
244 less pronounced than the Dente torrent.

245 At present, erosion and deposition within the torrent channels have yet to be estimated. Hence, the values indicated  
246 in Table 3 reflect a low range of eroded volumes. The topographic difference observed represents only the end  
247 state. During the event, one or more erosion phases may have occurred, significantly incising the heart of the  
248 torrents and generating a substantial sediment input. In some cases, certain zones correspond solely to channel  
249 aggradation without erosion. These nuances cannot be accurately quantified with our datasets, and sediment  
250 balances may be "distorted" as a result. Into the inner channel, significant erosion may occur, and a few hundred  
251 meters further downstream, erosion deposits may be found. Consequently, a zero balance may be observed when  
252 calculated on a GIS. To simplify our analysis, we have chosen to focus on erosion at the head of the catchment  
253 area (gullies, landslides) and the outlet (alluvial fan), as well as bank erosion when particularly pronounced. This

254 approach explains the limited additional information for the Morte, Para, and Scabrie valleys, as these torrents  
 255 likely generated more sediment.



256 *Fig. 5 : Spatial representation of mobilized volumes in the Viévoła watershed, including calculated erosion and deposition*  
 257 *areas based on the methodology outlined above. The geomorphological map (Figure 2) provides a plan view of the study area.*  
 258 *A) corresponds to the Dente torrent, B) the Rabay torrent, C) the Morte torrent, D) the Para torrent, and E) the Scabrie torrent.*  
 259 *Thin red line represent Viévoła catchment. The orange dots represent landslides that occurred during the event. The green*  
 260 *polygon represents the surface area of the Viévoła fan, estimated to be 250,000 m<sup>2</sup> using ArcGIS Pro. Erosion areas are*  
 261 *indicated by yellow to red dots, with their surfaces detailed in Table 3. Blue dots correspond to deposition on the Viévoła fan,*  
 262 *with an estimated surface area of 67,036 m<sup>2</sup>.*

263 The volume deposited at the Viévoła fan computed is 88 500 m<sup>3</sup> (Figure 5). This result aligns with the information  
 264 provided by the ONF and the RTM following Storm Alex, which estimates the volume of the Viévoła fan at 90 000  
 265 m<sup>3</sup> (ONF-RTM, ONF-DRN, and INRAE-ETNA, 2023).

266 The deposition area on the Viévoła fan covers 67 036 m<sup>2</sup> (Figure 5). When calculating the ratio of deposited  
 267 volume to surface area ( $V_{\text{deposited}} / \text{surface}$ ), we obtain that, on average, the area was engraved by 1.3 m across the  
 268 entire surface of the reactivated fan during the event, with very significant maxima reaching up to 9 meters in  
 269 height, as illustrated in the ONF-RTM, ONF-DRN, and INARE-ETNA report from 2023.

270 Across a total area of approximately 250 000 m<sup>2</sup> on the fan (Figure 2 and Figure 5), there are railway facilities,  
 271 bridges, residences, and a holiday camp. Roughly 26% of the fan area was reactivated by the mentioned torrents,  
 272 resulting in the engraving of buildings in the holiday camp (Figure 2). The SNCF (French National Railway  
 273 Company) bridge was also affected, contributing to the interruption of railway traffic to that area. Furthermore,  
 274 the expansion of the active band of the Roya River on the eastern part of the alluvial fan also played a role in  
 275 depositing/eroding a portion of it, leading to the destruction of bridges and roads. These advantageous reliefs, with  
 276 their gentle slopes in a particularly narrow valley, offer opportunities for land use. Traditional floods only  
 277 minimally affect or do not impact alluvial fans, leaving them inactive. However, during extreme events like Alex's,  
 278 a significant portion of fan surface was reactivated, causing destruction and cutting off access to the population.

279 Considering both produced and deposited sediments, the analysis reveals that more 90 000 m<sup>3</sup> were discharged  
280 into the Roya river. In relative terms, the sediment deposited was relatively small, contrasting with the substantial  
281 export into the Roya. These sediments have played a crucial role in significant erosions and morphological  
282 changes, impacting anthropogenic infrastructure along the entire stretch of the Roya River (approximately 60 km).  
283 This situation resulted several weeks of isolation for the affected valleys, necessitating states of emergency  
284 declarations.

## 285 6. Conclusions and perspectives

286 In conclusion, our study has highlighted the significance of the Viévol catchment area as a significant sediment  
287 source of sediment, with particular importance of the Dente and Rabay torrent heads. Erosion during the extreme  
288 storm event was most pronounced in areas characterised by scree and outwash fluvio-glacial deposits. Despite the  
289 lack of a high-quality Digital Terrain Model (DTM) before the event, our straightforward method, based on a  
290 Digital Surface Model (DSM) derived from autocorrelation of high-quality orthoimages, enabled us to estimate  
291 sediment volumes, both exported to the Roya River or deposited inside the Viévol catchment area. These results,  
292 provide valuable insights into the geomorphological response of slopes and rivers to extreme events. Extending  
293 our study to the entire Roya Valley holds the promise of deepening our understanding of factors that predispose  
294 mountainous areas to such events, triggers of extreme hydro-sedimentological events, and morphological changes  
295 that occur within catchment areas following significant incidents. Combining digital data with information  
296 collected during field campaigns conducted in March, June, and October 2023 can further enhance our  
297 understanding of the extreme water-sediment flow processes. This comprehensive approach will make it possible  
298 to characterize and model this type of extreme event, and thus to be better prepared to manage similar extreme  
299 events in the future.

## 300 Acknowledgements

301 We express our sincere gratitude to all those who have contributed to this research. The authors acknowledge the  
302 support of the ANR-17-CE03-004-01 project, the "coup de pouce" project of ISTeP Sorbonne University, and the  
303 doctoral fellowship from the French Research Ministry for funding this study. Additionally, we would like to  
304 extend our thanks to the Institute of Ocean and Environmental Transition of the Alliance Sorbonne University for  
305 financing three field campaigns. We are grateful to the Monastery of Saorge (Center for National Monuments) for  
306 providing accommodation for researchers. We also recognize the MITI of CNRS for funding the equipment used  
307 in this study. Finally, our appreciation goes to Nicoletta BIANCHI from the Musée des Merveilles in Tende (Alpes-  
308 Maritimes department) for her invaluable assistance in the field. I express my gratitude to the two reviewers whose  
309 constructive comments have significantly enhanced the quality of this work.

310

311

312

313

314

315

316

317

318

319

320

321 Blanchard, R. (1949) 'Tome cinquième : les Grandes Alpes françaises du Sud', in *Les Alpes occidentales*.  
322 Grenoble et Paris: Arthaud, p. 514.

- 323 Brisset, E. *et al.* (2015) 'Lateglacial/Holocene environmental changes in the Mediterranean Alps inferred from  
324 lacustrine sediments', *Quaternary Science Reviews*, 110, pp. 49–71. Available at:  
325 <https://doi.org/10.1016/j.quascirev.2014.12.004>.
- 326 Carrega, P. and Michelot, N. (2021) 'Une catastrophe hors norme d'origine météorologique le 2 octobre 2020  
327 dans les montagnes des Alpes-Maritimes', *Physio-Géo*, (Volume 16), pp. 1–70. Available at:  
328 <https://doi.org/10.4000/physio-geo.12370>.
- 329 Cerema (2021) *RETEX technique ALEX - Inondations des 2 et 3 octobre 2023. consensus hydrologique -*  
330 *Unpublished report - CEREMA*, p. 59.
- 331 Derrien, M. *et al.* (1992) 'Classification de la végétation sur la France à l'aide de l'AVHRR de NOAA-11',  
332 *Noréis*, t. 39(155), pp. 269–282.
- 333 Gèze, B. and Nesteroff, N. (1996) *Carte géologique de la France à 1/50 000. Feuille : 973 - Menton - Nice.*  
334 Orléans: Editions du BRGM.
- 335 Holben, B.N. (1986) 'Characteristics of maximum-value composite images from temporal AVHRR data',  
336 *International Journal of Remote Sensing*, 7(11), pp. 1417–1434. Available at:  
337 <https://doi.org/10.1080/01431168608948945>.
- 338 IGN (2018) *RGE ALTI® Version 2.0 - Descriptif de contenu*, p. 37.
- 339 IGN (2020) *Un avion de l'IGN photographie les zones sinistrées, un avion de l'IGN photographie les zones*  
340 *sinistrées*. Available at: [https://www.ign.fr/institut/nos-domaines-d'intervention/prevention-des-risques/tempe-](https://www.ign.fr/institut/nos-domaines-d'intervention/prevention-des-risques/tempe-alex-un-avion-de-lign-photographie-les-zones-sinistrees)  
341 [alex-un-avion-de-lign-photographie-les-zones-sinistrees](https://www.ign.fr/institut/nos-domaines-d'intervention/prevention-des-risques/tempe-alex-un-avion-de-lign-photographie-les-zones-sinistrees).
- 342 IGN (2021) *Lidar HD : vers une nouvelle cartographie 3D du territoire, Lidar HD : vers une nouvelle*  
343 *cartographie 3D du territoire*. Available at: [https://www.ign.fr/institut/lidar-hd-vers-une-nouvelle-cartographie-](https://www.ign.fr/institut/lidar-hd-vers-une-nouvelle-cartographie-3d-du-territoire)  
344 [3d-du-territoire](https://www.ign.fr/institut/lidar-hd-vers-une-nouvelle-cartographie-3d-du-territoire).
- 345 IGN (2023) *MNS Correl Version 1.0 - Descriptif de contenu*. French National Institute of Geography, p. 12.
- 346 Julian, M. (1980) *Les Alpes maritimes franco-italiennes: étude géomorphologique*. Université de Lille III.
- 347 Julian, M. (1997) 'Les glaciations des Alpes Maritimes : essai de mise au point.', in *Géo-Méditer :*  
348 *Géographique physique et méditerranée*. Editions de la Sorbonne, pp. p245-261.
- 349 Liébault, F. *et al.* (2024) 'Channel change during catastrophic flood: Example of Storm Alex in the Vésubie and  
350 Roya valleys', *Geomorphology*, 446, p. 109008. Available at: <https://doi.org/10.1016/j.geomorph.2023.109008>.
- 351 ONF-RTM, ONF-DRN, and INRAE-ETNA (2023) 'Retour d'expérience technique de la crue du 2 octobre 2020  
352 dans la vallée de la Roya - Volet torrentiel'. Recherche Data Gouv. Available at:  
353 <https://doi.org/10.57745/B69M2O>.
- 354